

Towards modelling the central engine of short GRBs

José A. Font¹, Luciano Rezzolla², Bruno Giacomazzo^{3,4}, Luca Baiotti⁵, David Link⁶

¹ Departamento de Astronomía y Astrofísica, Universitat de València, 46100 Burjassot (Valencia), Spain

² Max-Planck-Institut für Gravitationsphysik, Albert-Einstein-Institut, Potsdam-Golm, Germany

³ Department of Astronomy, University of Maryland, College Park, MD, USA

⁴ Gravitational Astrophysics Laboratory, NASA Goddard Space Flight Center, Greenbelt, MD USA

⁵ Institute of Laser Engineering, Osaka University Yamada-oka 2-6, Suita, Osaka 565-0871, Japan

⁶ Institut für Physik, Humboldt-Universität zu Berlin, Berlin, Germany

E-mail: j.antonio.font@uv.es

Abstract. Numerical relativity simulations of non-vacuum spacetimes have reached a status where a complete description of the inspiral, merger and post-merger stages of the late evolution of close binary neutron systems is possible. Determining the properties of the black-hole-torus system produced in such an event is a key aspect to understand the central engine of short-hard gamma-ray bursts (sGRBs). Of the many properties characterizing the torus, the total rest-mass is the most important one, since it is the torus' binding energy which can be tapped to extract the large amount of energy necessary to power the sGRB emission. In addition, the rest-mass density and angular momentum distribution in the torus also represent important elements which determine its secular evolution and need to be computed equally accurately for any satisfactory modelling of the sGRB engine. In this paper we summarize our recent results from fully general-relativistic simulations of the coalescence of unequal-mass binary neutron stars, whose evolution is followed through the inspiral phase, the merger and prompt collapse to a black hole, up until the appearance of a thick accretion disk, which is studied as it enters a regime of quasi-steady accretion. Our simulations show that large-scale, quasi-Keplerian tori with masses as large as $\sim 0.2 M_{\odot}$ can be produced as the result of the inspiral and merger of binary neutron stars with unequal masses.

1. Introduction

Simulating the merger of binary neutron stars in general relativity has been a long-term major target of numerical relativity. Progress has been steady, owing to the difficulties imposed by the presence in such setting of strong gravitational and magnetic fields, shock waves, and matter motion at relativistic speeds. In addition, the multidimensional character of the scenario and the formation of curvature singularities as a plausible outcome of the merger, have also conspired to slow down progress. Nevertheless, considerable advances have been achieved in recent years due to major developments in several key aspects of the problem, such as the formulation of the equations and the incorporation of equations of state (EOS) from nuclear physics. Likewise, the use of high-resolution numerical methods and adaptive mesh refinement, along with increased

computational resources, have also permitted to perform the simulations to significant levels of accuracy. A view of the state-of-the-art in the field is offered by the works of [1, 2, 3, 4, 5, 6, 7, 8, 9]

The characterization of the gravitational radiation produced in such mergers is one of the prime motivations behind the simulations. Such events are among the most promising sources of detectable gravitational radiation for laser interferometric detectors. Current estimates for the detection rate relative to first-generation detectors is ~ 1 event per $\sim 40 - 300$ years, increasing to an encouraging $\sim 10 - 100$ events per year for the advanced detectors [10]. The second motivation to simulate binary neutron star mergers is establishing whether the end-product of the merger can operate as the central engine of short-hard gamma-ray bursts (sGRBs) [11, 12]. Depending on the suitability of the model parameters, existing simulations show the formation of a stellar mass black hole surrounded by a hot disk. Driven by neutrino processes and magnetic fields, such a compact system may indeed be capable of launching a relativistic fireball with an energy of $\sim 10^{48}$ erg on a timescale of $0.1 - 1$ s [13].

In this paper we present a summary of our recent efforts in the simulation of binary neutron star mergers. Full details of these simulations were given in [9] to which the interested reader is addressed for a complete account of our study. In particular, we present here the results for only two models, and focus our discussion on the late-time dynamics of the torus formed after the merger of such two unmagnetized, equal- and unequal-mass neutron star binaries. As reported in [9] our simulations indicate that large-scale tori with masses as large as $\sim 0.2 M_{\odot}$ can be produced as the result of the inspiral and merger of binary neutron stars with unequal masses. These tori are typically of large size, with quasi-Keplerian distribution of angular momenta, showing quasi-stationary evolutions and the absence of dynamical instabilities. Furthermore, the gravitational-wave emission reveals that the waveforms are sensitive to the mass ratio in the binary, both during the inspiral and after the merger, and could be used to extract important information on the structure and EOS of the progenitor stars.

2. Physical and computational framework

The basic set of equations we solve for the simulations reported in this work includes the equations describing the dynamics of the gravitational field (the Einstein equations) and the equations describing the dynamics of the matter. The Einstein equations are formulated following the conformal traceless BSSN formalism with a “1 + log” slicing condition and a “Gamma-driver” shift condition (the interested reader is addressed to [14] for a detailed discussion of the equations and gauges used). These equations are solved using the **CCATIE** code, a three-dimensional finite-differencing code. Correspondingly, the general-relativistic hydrodynamics equations are solved using the **Whisky** code [15], which adopts a flux-conservative formulation of the equations as presented in [16] and high-resolution shock-capturing schemes. For the simulations we employ an ideal fluid EOS, in which the pressure p is expressed as $p = \rho \epsilon (\Gamma - 1)$, where ρ is the rest-mass density, ϵ is the specific internal energy, and Γ is the adiabatic exponent. The value chosen for the latter is $\Gamma = 2$. As in [3], the gravitational-wave signal is extracted using two independent methods, on the one hand a method based on the Newman-Penrose formalism and, on the other hand, a method based on the measurements of the non-spherical gauge-invariant perturbations of a Schwarzschild black hole. The hierarchy of the computational grid, one of the most important aspects of the simulations, is handled by the **Carpenter** mesh refinement driver [17]. We use six refinement levels with a 2 : 1 refinement factor for successive levels. The timestep on each grid is set by the Courant condition and, hence, by the spatial grid resolution for that level; the typical CFL coefficient is set to 0.35. The time evolution is carried out using a 4th-order-accurate Runge-Kutta integration algorithm. Boundary data for finer grids are calculated with spatial prolongation operators employing 3rd-order polynomials and with prolongation in time employing 2nd-order polynomials. Initially, the number of grid points across the star is ~ 100 . The torus surrounding the black hole after

the merger is usually not contained within the finest grid, but its high-density region is covered by the second finest grid with resolution $\Delta_2 = 0.3$. The whole grid is set up to be symmetric with respect to the (x, y) plane. The boundary conditions are chosen to be radiative for the metric, in order to prevent gravitational waves from scattering back into the grid, and static for the hydrodynamical variables.

We use quasi-equilibrium initial data generated with the multi-domain spectral-method code LORENE developed at the Observatoire de Paris-Meudon [18]. A full list of all considered models together with a selection of physical quantities defining them, *e.g.* baryon mass and ADM mass, orbital frequency and initial angular momentum, etc., is given in [9]. (The models of the lowest mass ratios in Ref. [9] were kindly provided by Dorota Gondek-Rosińska.) Here, as mentioned in the Introduction, we only focus in two representative models of the sample discussed in [9], as these highlight the differences in the evolution of equal-mass and unequal-mass binaries. Following the notation of [9] we label these two models M3.6q1.00 and M3.4q0.70, respectively. The first one is an equal-mass model (mass ratio $q = 1$) with total baryonic mass $M_{\text{tot}} = 3.6M_{\odot}$ and the second one is an extreme unequal-mass model ($q = 0.7$) with total baryonic mass $M_{\text{tot}} = 3.4M_{\odot}$.

3. Results

Figure 1 shows a selection of representative isodensity contours on the equatorial plane for both models. At the initial time (top panel), the stars are in their quasi-equilibrium configuration at a coordinate separation of 45 km. The asymmetry of model M3.4q0.70 before the evolution starts is already apparent. The more massive star is much more compact than its extended companion, which is deformed already at the initial distance by tidal forces. Along the evolution of model M3.6q1.00 (see [9]), matter is ejected in small amounts during the inspiral phase and in larger amounts during the merger phase, when shock waves resulting from the collision are much stronger. On the contrary, model M3.4q0.70 is characterized by the formation of large spiral arms extending well beyond the domain shown in the figure, which are responsible for the rapid ejection of matter. Therefore, for model M3.4q0.70, gravitationally bound matter travelling along the spiral arms away from the central object will form a more massive accretion torus around the central black hole than that formed in the case of an equal-mass, symmetric binary system.

For model M3.6q1.00, the mass and spin of the black hole measured at formation are $M = 2.56 M_{\odot}$ and $a \equiv J/M^2 = 0.745$, values which barely change throughout the subsequent evolution of the system. These quantities could not be measured accurately for model M3.4q0.70 (see [9] for details). The recoil velocity imparted to the black hole at the end of the inspiral phase are respectively 0.28 km/s for model M3.6q1.00 and 15.82 km/s for model M3.4q0.70. While such recoil velocities are much smaller than those measured for binary black holes, they could still yield astrophysically interesting results being comparable or larger than the escape velocity from the core of a globular cluster, $v_{\text{esc}} \sim 50$ km/s [19].

The middle panels of figure 1 correspond to the time when the system enters the regime of quasi-stationary accretion (QSA) shortly after the formation of the black hole, while the bottom two panels refer to the final time of the evolution. We define the onset of the QSA as the time when the condition $\dot{M}_{\text{tot}}/M_{\text{tot}} < 10^{-6}(Gc^{-3}M_{\odot})^{-2}$ is satisfied for the first time, where M_{tot} is the total mass of the binary and \dot{M}_{tot} is the mass accretion rate, defined as $\dot{M}_{\text{tot}} = \frac{d}{dt} \int \rho W \sqrt{\gamma} d^3x$, where W is the Lorentz factor and γ is the determinant of the spatial metric. In addition, figure 2 shows color-coded contours of the rest-mass density for both models in the (x, z) plane. Taken together, these two figures allow for a closer view of the morphological features of the forming disks, in particular, their spatial dimension and thickness. The morphological differences between both models are significant. The equal-mass model produces a highly symmetric, geometrically thin disk, similar to the ones already observed

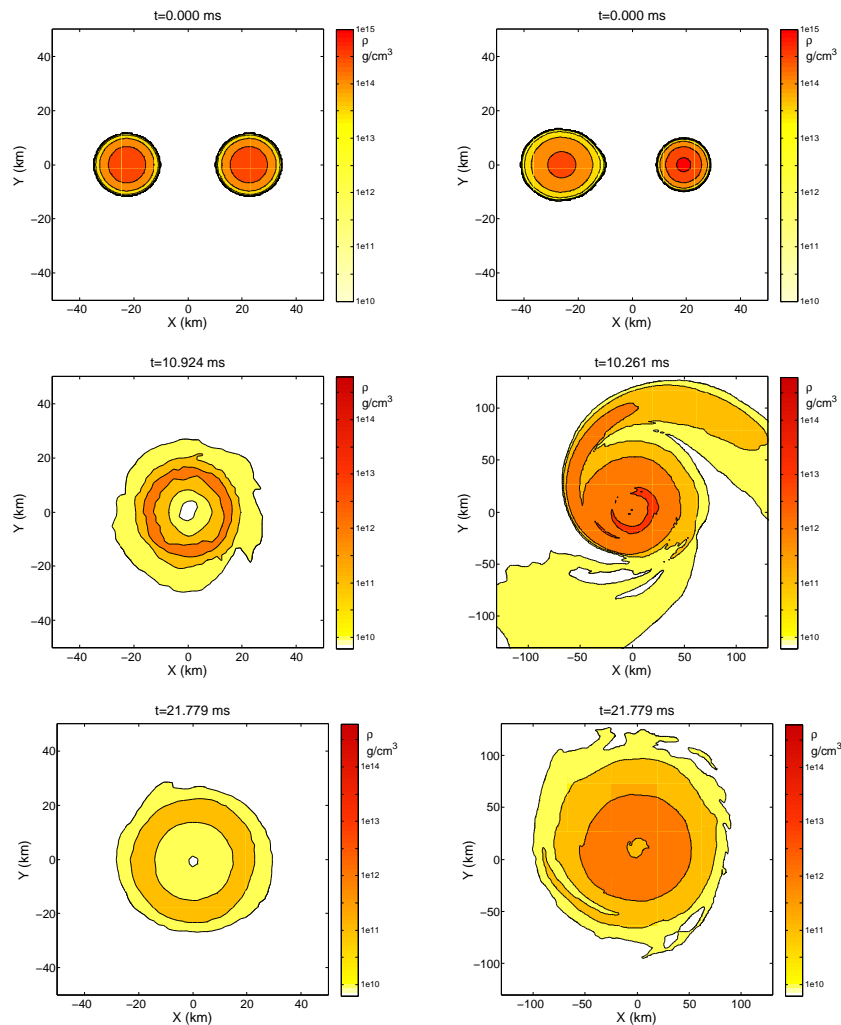


Figure 1. Isodensity contours for models M3.6q1.00 (left) and M3.4q0.70 on the (x, y) plane. The top panels show the binaries at $t = 0$ to highlight the asymmetry of the unequal-mass model. The times when the frames have been taken are shown on top while the color-code for the rest-mass density is indicated to the right of each plot. The middle panels show the morphology of the tori at the onset of the quasi-stationary accretion, while the bottom panels correspond to the end of the simulation. Note the change in the scale of the plots of the last two panels of model M3.4q0.70.

for other equal-mass initial data in [3]. The unequal-mass model, on the other hand, at the time of the onset of the regime of QSA is characterized by the presence of a large spiral arm, which has not yet been accumulated onto the central disk surrounding the formed black hole. The diameters of the disks and their vertical heights differ in a significant way between the two models: at the end of the evolution and using the $\rho = 10^{10} \text{ g/cm}^3$ isodensity contour as the reference value below which material is not considered part of the disk, our simulations yield disk diameters of $\sim 50 \text{ km}$ for model M3.6q1.00 and $\sim 150 \text{ km}$ for model M3.4q0.70. The corresponding vertical scale is $\sim 5 \text{ km}$ and $\sim 35 \text{ km}$, respectively. While the tori differ in size by a factor ~ 3 , they differ by a factor ~ 200 in mass while having comparable mean rest-mass densities.

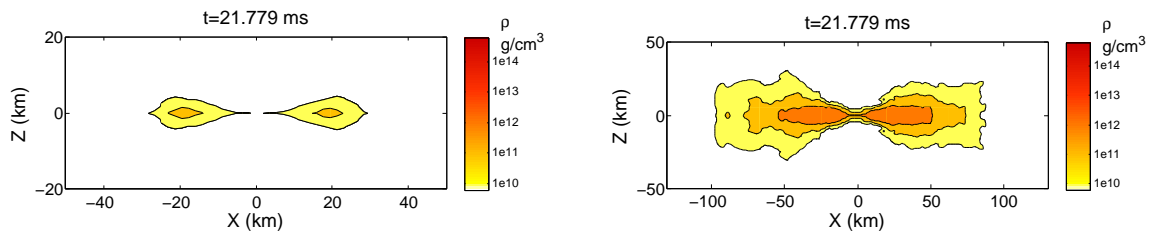


Figure 2. Isodensity contours for models M3.6q1.00 (left panel) and M3.4q0.70 showing the morphology of the tori at the end of the simulation on the (x, z) plane. Note that the disks in the two panels have very different lengthscales. The thickness of the disk for the unequal-mass binary is apparent.

The violent dynamics of the merger process is reflected on an associated large emission of gravitational radiation. This issue was discussed in [9], to which the interested reader is addressed for further specific details. The main result of our findings is that present gravitational-wave detectors are unlikely to detect any of the binaries of our sample if they are located at a distance of 100 Mpc and observed only during the final part of the inspiral. However, advanced detectors will be able to reveal these sources even at large distances and measure them with significant SNRs in the case of third-generation detectors such as the Einstein Telescope [20].

In agreement with previous simulations by [1], we have found that the smaller the mass ratio q of the binary the larger the mass of the resulting accretion disk. It should be noted that the definition of what constitutes a torus and, thus, what is its mass is rather arbitrary. This is due to the fact that, after the apparent horizon has formed, a substantial part of the rest-mass lies still outside, although it will accrete rapidly onto the black hole. Given this arbitrariness, we define the torus mass M_{tor} as the total rest mass outside the apparent horizon when the disk enters the QSA regime, a regime which is found in all models investigated in [9]. With this definition we find that while the equal-mass model produces a disk of barely $10^{-3} M_{\odot}$, model M3.4q0.70 produces significantly more massive tori with masses of about $0.2 M_{\odot}$. A phenomenological expression for the torus mass was derived in [9] (see also [1]), which showed that tori with masses up to $\sim 0.35 M_{\odot}$, are possible for mass ratios $q \sim 0.75 - 0.85$. These values are well above the typical lower bounds discussed in the context of short GRBs triggered by thermal energy deposition above the poles of the black hole by $\nu\bar{\nu}$ annihilation [21].

In [9] spacetime diagrams for observers comoving with the black hole were used to analyze the evolution of the tori and to gain some insight on their dynamics. An example is shown in figure 3, which displays the evolution of the color-coded rest-mass density embedded in a spacetime diagram with the $x - x_{\text{AH}}$ coordinate on the horizontal axis, where x_{AH} is the position of the apparent horizon, and the coordinate time t on the vertical axis. By comparing both diagrams it is again evident the striking difference in the evolution of both models. On the one hand, the equal-mass model shows a global oscillatory movement with respect to the location of the black hole horizon. On the other hand, the spacetime diagram for the density evolution of model M3.4q0.70 shows very rapid expansions corresponding to the ejection of the large spiral waves mentioned before. As discussed by [9], most of this matter is still bound, as the criterion $u_t > -1$ is fulfilled, but it nevertheless reaches distances which are several hundreds of km away from the black hole, leading to tori that have spatial dimensions as large as ~ 80 km. This matter will eventually fall back onto the tori, where it may lead to enhanced accretion and consequently to a new and *delayed* gamma-ray emission as the one recently observed in [22].

The stability of the tori resulting from binary neutron star mergers is a central issue for current models of GRBs. Any instability which might disrupt the black hole plus thick disk

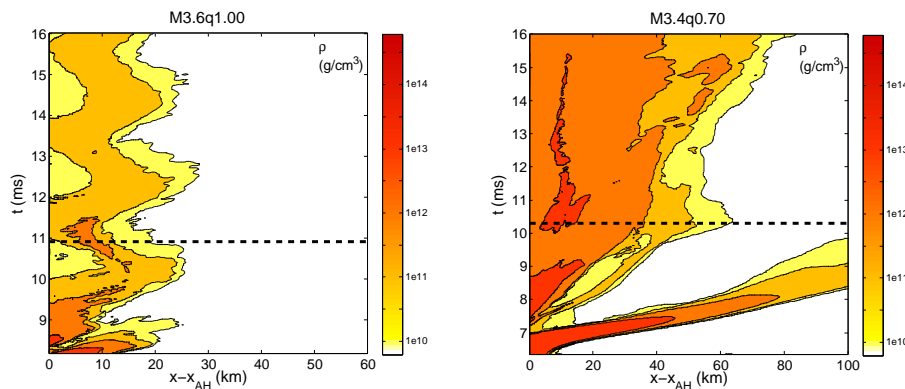


Figure 3. Evolution of the rest-mass density ρ for models M3.6q1.00 (left) and M3.4q0.70 along the positive x axis in a frame comoving with the BH. The panels show the color-coded rest-mass density embedded in a spacetime diagram with the $(x - x_{\text{AH}})$ coordinate on the horizontal axis, being x_{AH} the position of the apparent horizon, and the coordinate time t on the vertical axis. For each model, the dotted horizontal line marks the onset of the regime of QSA.

system on timescales shorter than the duration of the energy release by the GRB source could pose a severe problem for the prevailing models. One such instability is the so-called runaway instability [23]. General relativistic hydrodynamical simulations of such instability were first performed by [24, 25, 26, 27], who treated the dynamics of the gravitational field in an approximate way and neglected the self-gravity of the torus. These investigations concluded that tori with constant distribution of specific angular momentum were unstable while non-constant (power-law) angular momentum disks were stable. More recently, in [28] the first simulations in full general relativity of marginally-stable self-gravitating tori in axisymmetry were presented. The purpose of this work was to evaluate the influence of the torus self-gravity on the runaway instability. The results of [28] indicate that tori are indeed stable irrespective of the angular momentum distribution. Our simulations, summarized in the spacetime diagrams of figure 3, which are not restricted to axisymmetry but are however constrained to much shorter timescales, reach the same conclusion: Self-gravitating tori around black holes, as those produced by the merger of binary neutron stars, are stable at least on the dynamical timescales investigated here. Further evidence has been recently collected by [29] where different types of non-axisymmetric instabilities of self-gravitating disks have been investigated. It is also worth pointing out that in the case of *magnetized* binary neutron star mergers, the resulting disks could be however unstable to the magneto-rotational instability [30].

The global oscillations of the equal-mass model shown in the left panel of the spacetime diagram of figure 3 are also found in the mass accretion rate, a quantity which is central to estimate the lifetime of the disk and which was shown in [9] to be subject to quasi-periodic oscillations as the torus moves in and out at about the radial epicyclic frequency. The mass flux of the unequal-mass model, on the other hand, is found to be rather constant in time, a fact which reflects a very different distribution of angular momentum in the tori. The profiles of the specific angular momentum $\ell \equiv -u_\phi/u_t$ along the x -axis are displayed in the left panel of figure 4, for the tori produced by the two models (model M3.6q1.00, blue lines extending to ~ 20 km; model M3.4q0.70, red lines extending up to ~ 70 km). The profiles are computed in a frame comoving with the black hole and for densities $\rho > 10^{10}$ g/cm³. Quite clearly, the specific angular momentum decreases outward at all times for the equal-mass binary, while it increases outward for the unequal-mass one (although it was initially decreasing at the innermost

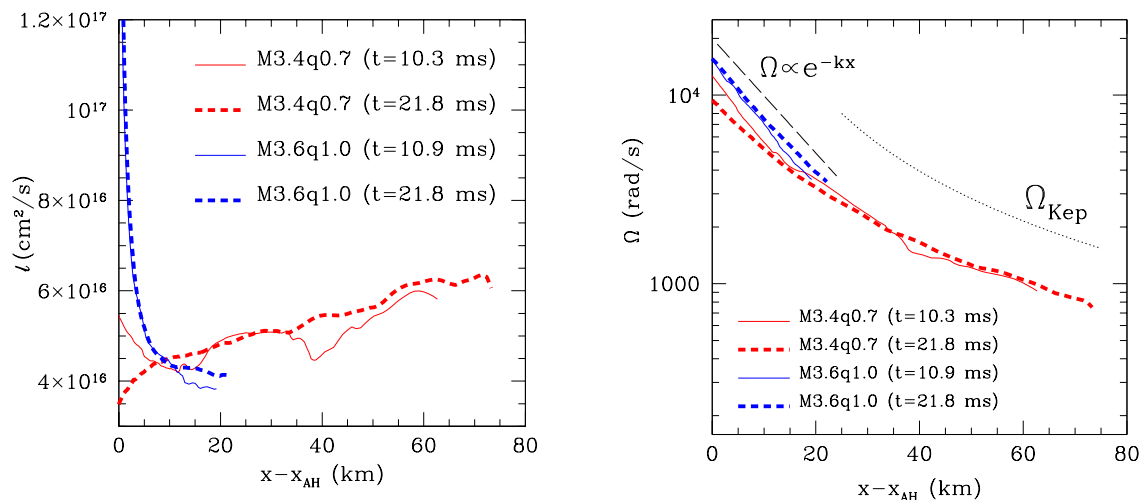


Figure 4. Profiles along the x -axis of the specific angular momentum (left) and angular velocity (right) of the tori produced by the two binaries considered. Different line types refer either to the onset of the QSA ($t \sim 10$ ms, thin solid lines) or to the end of the simulation ($t \sim 22$ ms, thick dashed lines). Left plot: Note the different profiles present in both models and that the specific angular momentum for the unequal-mass case increases outwards. Right plot: the dotted line indicates the reference Keplerian angular velocity, which matches very well the outer parts of the torus from the unequal-mass binary. The long-dashed line is an exponentially decaying profile, which instead reproduces well the profile for the equal-mass binary.

parts). Rayleigh's criterion for dynamical stability is clearly satisfied by model M3.4q0.70 but it is equally-clearly violated by model M3.6q1.00, which is nevertheless stable. The reason for this could be due to the fact that Rayleigh's criterion assumes stationary and purely azimuthal motion, a condition which is not satisfied for the unequal-mass binary, which shows instead large radial epicyclic oscillations.

Correspondingly, the right panel of figure 4 shows the profiles of the angular velocity Ω along the x -axis for the tori produced by our two models. While the equal-mass binary has an exponentially decaying profile (long-dashed line), $\Omega \propto \exp[-k(x - x_{\text{AH}})] \sim \exp[-0.07(x - x_{\text{AH}})]$, which does not change significantly with time, the unequal-mass binary reaches at the end of the simulation a profile which is, especially in the outer parts, essentially Keplerian, with $\Omega_{\text{Kep}} \sim x^{-3/2}$ (dotted line). This feature explains the scaling of the specific angular momentum as $\ell \sim x^{1/2}$ and provides firm evidence that the tori produced in this case will be dynamically stable.

4. Summary

We have presented results from a subset of simulations of binary neutron star mergers reported in [9]. Our discussion has been focused on the late-time dynamics of the torus formed after the merger of two unmagnetized, equal- and unequal-mass neutron star binaries. The evolution of the neutron stars has been followed through the inspiral phase, the merger and prompt collapse to a black hole, up until the appearance of an accretion disk, which has been studied as it enters and remains in a regime of quasi-steady accretion.

We have found that the torus mass increases with the initial mass asymmetry of the neutron stars. Equal mass binaries with a total baryonic mass larger than $3.7 M_{\odot}$ lead to prompt black hole formation and produce tori with radial extension of ~ 30 km and with masses $\sim 10^{-3} M_{\odot}$. On the contrary, unequal-mass binaries produce significantly more massive tori with masses of

about $0.2M_{\odot}$. The associated tori are also much more extended with typical sizes ~ 150 km. A phenomenological expression for the torus mass derived in [9] showed that tori with masses up to $\sim 0.35 M_{\odot}$ are possible.

The torus dynamics is remarkably different for the equal- and unequal-mass binaries. While tori from equal-mass binaries exhibit a quasi-periodic form of accretion associated with the radial epicyclic oscillations of the disks, those from unequal-mass binaries exhibit a quasi-steady form of accretion. In addition, the analysis of the distribution of the angular momentum in the tori has shown no evidence for the development of non-axisymmetric instabilities. Angular momentum is transported outwards more efficiently for smaller values of the mass asymmetry, yielding Keplerian angular velocity distributions. As discussed in detail in [9], advanced gravitational wave detectors will be able to reveal these sources at large distances (~ 100 Mpc) and measure them with significant signal-to-noise ratios.

Acknowledgments

We are grateful to the Meudon group and to D. Gonddek-Rosińska for producing some of the initial data used in the calculations reported in [9] which form the basis for the results of this paper. Additional gratitude goes to Gian Mario Manca, E. Schnetter and all the *Carpet/Cactus* developers. The computations were performed on the Damiana cluster at the AEI, on the MareNostrum cluster at the Barcelona Supercomputing Center and on the Ranger cluster at the Texas Advanced Computing Center through TERAGRID allocation TG-MCA02N014. This work was supported in part by the DFG grant SFB/Transregio 7, by “CompStar”, a Research Networking Programme of the European Science Foundation, by the JSPS Postdoctoral Fellowship For Foreign Researchers, Grant-in-Aid for Scientific Research (19-07803), and by the Spanish Ministerio de Educación y Ciencia (AYA 2007-67626-C03-01).

References

- [1] Shibata M and Taniguchi K 2006 *Phys. Rev. D* **73** 064027
- [2] Anderson M *et al.* 2008 *Phys. Rev.* **D77** 024006
- [3] Baiotti L, Giacomazzo B and Rezzolla L 2008 *Phys. Rev. D* **78** 084033
- [4] Anderson M, Hirschmann E W, Lehner L, Liebling S L, Motl P M, Neilsen D, Palenzuela C and Tohline J E 2008 *Phys. Rev. Lett.* **100** 191101
- [5] Baiotti L, Giacomazzo B and Rezzolla L 2009 *Class. Quantum Grav.* **26** 114005
- [6] Liu Y T, Shapiro S L, Etienne Z B and Taniguchi K 2008 *Phys. Rev. D* **78** 024012
- [7] Giacomazzo B, Rezzolla L and Baiotti L 2009 *MNRAS* **399** L164–L168
- [8] Kiuchi K, Sekiguchi Y, Shibata M and Taniguchi K 2009 *Phys. Rev. D* **80** 064037
- [9] Rezzolla, L, Baiotti, L, Giacomazzo, B, Link, D and Font, J.A. 2010, *Class. Quantum Grav.* **27** 114105
- [10] Belczynski K, Taam R E, Kalogera V, Rasio F and Bulik T 2007 *Astrophysical Journal* **662** 504
- [11] Narayan R, Paczynski B and Piran T 1992 *Astrophys. J.* **395** L83
- [12] Zhang B and Meszaros P 2004 *Int. J. Mod. Phys. A* **19** 2385
- [13] Piran T 2004 *Rev. Mod. Phys.* **76** 1143–1210
- [14] Baiotti L, Hawke I and Rezzolla L 2007 *Class. Quantum Grav.* **24** S187–S206
- [15] Baiotti L, Hawke I, Montero P J, Löffler F, Rezzolla L, Stergioulas N, Font J A and Seidel E 2005 *Phys. Rev. D* **71** 024035
- [16] Banyuls F, Font J A, Ibáñez J M, Martí J M and Miralles J A 1997 *Astrophys. J.* **476** 221
- [17] Schnetter E, Hawley S H and Hawke I 2004 *Class. Quantum Grav.* **21** 1465–1488
- [18] Gourgoulhon E, Grandclément P, Taniguchi K, Marck J A and Bonazzola S 2001 *Phys. Rev. D* **63** 064029
- [19] Webbink R F 1985 *Dynamics of Star Clusters (IAU Symposium vol 113)* ed J Goodman & P Hut pp 541–577
- [20] Einstein Telescope <http://www.et-gw.eu>
- [21] Oechslin R and Janka, H-Th 2006 *Astron. Astrophys.* **368**, 1489–1499
- [22] Giuliani A and others 2010 *Astrophys. J.* **708** L84–L88
- [23] Abramowicz M A, Calvani M and Nobili L 1983 *Nature* **302** 597–599
- [24] Font J A and Daigne F 2002 *MNRAS* **334** 383–400
- [25] Font J A and Daigne F 2002 *Astrophys. J.* **581** L23–L26
- [26] Zanotti O, Rezzolla L and Font J A 2003 *Mon. Not. Roy. Soc.* **341** 832

- [27] Daigne F and Font J A 2004 *MNRAS* **349** 841–868
- [28] Montero P J, Font J A and Shibata M 2010 *Phys. Rev. Lett.* **104** 191101
- [29] Korobkin O, Abdikamalov E, Schnetter E, Stergioulas N and Zink B 2010 arXiv:1011.3010
- [30] Giacomazzo B, Rezzolla L and Baiotti L 2010 *arXiv:1009.2468*